Available online at www.sciencedirect.com
ScienceDirect
Catalysis Today 136 (2008) 173–182
CATALYSIS TODAY
www.elsevier.com/locate/cattod

Sulfur and temperature effects on the spatial distribution of reactions inside a lean NO_x trap and resulting changes in global performance

Jae-Soon Choi *, William P. Partridge, Josh A. Pihl, C. Stuart Daw

Fuels, Engines, and Emissions Research Center, Oak Ridge National Laboratory, P.O. Box 2008, MS-6472, Oak Ridge, TN 37831-6472, USA

Available online 4 March 2008

Abstract

We experimentally studied the influence of temperature and sulfur loading on the axial distribution of reactions inside a commercial lean NO_x trap (LNT) catalyst to better understand the global performance trends. Our measurements were made on a monolith core, bench-flow reactor under cycling conditions (60-s lean/5-s rich) at 200, 325, and 400 °C with intra-catalyst and reactor-outlet gas speciation. Postmortem elemental and diffuse reflectance infrared Fourier transform spectroscopy (DRIFTS) analyses of the catalyst also supplemented our gas species measurements. For the unsulfated catalyst, the NO_x storage/reduction (NSR) reactions were localized in the front (upstream) portion of the monolith, whereas oxygen storage/reduction reactions were distributed more evenly along the entire catalyst length. As a result, two axially distinct reaction zones were developed inside the working catalyst: an upstream ''NSR zone'' where both NO_x and oxygen storage/reduction took place and a downstream oxygen storage capacity (OSC)-only zone where the NSR reactions did not penetrate. The NSR zone involved less than half the LNT at 325 and 400 °C, but it included almost the entire length at 200 °C. Sulfation poisoned both the NSR and OSC reactions beginning at the catalyst upstream edge, with the NSR degradation occurring more rapidly and distinctly than the OSC. As sulfation proceeded, a third zone (the sulfated zone) developed and the NSR zone moved downstream, with a concomitant decrease in both the OSC-only zone and global NO_x conversion. The sulfation impact on NO_x conversion was greatest at 200 °C, when the NSR zone was largest. Ammonia selectivity increased with sulfation, which we attributed to a shortened OSC-only zone and resultantly reduced consumption of NH_3, slipping from the NSR zone, by downstream OSC. Lower temperatures also increased NH_3 selectivity. Nitrous oxide selectivity also increased with decreasing temperature but showed little dependence on sulfation. We proposed explanations for these trends in NH_3 and N_2O selectivity based on shifts in competing reaction rates in the three zones.
Published by Elsevier B.V.

Keywords: Lean NO_x trap; NO_x storage/reduction; Oxygen storage capacity; Sulfation; Temperature effect; Ammonia; Spatial distribution of reactions

1. Introduction

The excellent fuel economy of lean-burn engines has a high potential for reducing fossil fuel consumption and greenhouse gas emissions in the transportation sector. However, reduction of nitrogen oxides ($NO_x = NO + NO_2$) under oxidizing conditions poses a significant technical challenge to the automakers who need to meet increasingly stringent emission standards [1,2]. While well-established 3-way catalysts can efficiently remove NO_x from stoichiometric gasoline engines, they are ineffective under net oxidizing lean-burn conditions due to competition between O_2 and NO_x for limited reductants. Lean NO_x trap (LNT) catalysts (also known as NO_x storage/reduction or NSR catalysts) circumvent this issue by combining NO_x storage components (in general, alkali or alkaline earth metal) with supported precious metals similar to 3-way catalysts [3–6]. Under typical lean exhaust conditions, LNTs reversibly store NO_x as nitrates or nitrites (storage step). As the extent of NO_x storage reaches a pre-determined level, the exhaust is switched to a rich condition to release and reduce the stored NO_x (regeneration step).

LNTs are considered one of the promising lean NO_x aftertreatment options to meet upcoming regulations [1,2,6,7] and are being introduced to the market for both lean-burn gasoline [6] and diesel vehicles [2]. However, further technological improvements are needed to successfully implement LNTs across a broad range of applications, especially with regard to catalyst durability issues. Two major degradation mechanisms

* Corresponding author. Tel.: +1 865 946 1368; fax: +1 865 946 1354.
E-mail address: choijs@ornl.gov (J.-S. Choi).

0920-5861/$ – see front matter. Published by Elsevier B.V.
doi:10.1016/j.cattod.2008.01.008

for LNTs are sulfur poisoning and thermal aging [3]. Sulfur poisoning occurs through a pathway similar to NO_x storage: SO_2 in the engine exhaust is oxidized on precious metal sites and stored in conjunction with the alkali or alkaline earth metals in the washcoat. Sulfur can also bind to other LNT constituents such as the alumina support and oxygen storage components [8,9]. As sulfates are more stable than nitrates, sulfur accumulates over time and blocks the formation of nitrates. Therefore, a periodic desulfation step is needed to free up sites for NO_x storage. Generally, desulfation requires temperatures much higher than normal LNT operation, and can thus cause thermal aging with associated permanent performance loss [10,11]. Moreover, the high temperatures required for desulfation increase the fuel penalty of catalyst operation. An on-going technical challenge is therefore to develop more robust LNTs and efficient operating strategies to maintain high LNT performance with minimum fuel penalty. This development requires an improved fundamental understanding of sulfation and desulfation mechanisms and their impacts on various LNT reactions such as NO_x storage, oxygen storage, reductant consumption, and by-product formation along the monolith.

Ammonia breakthrough has been observed during LNT regeneration under various conditions [12–22]. While NH_3 is undesirable for LNT-only NO_x control systems, it can be useful as a reductant when combined with downstream NH_3-SCR (selective catalytic reduction) catalysts [22]. In practical implementation of either LNT system, it is important to accurately predict NH_3 breakthrough transients. Consequently, it is necessary to understand how NH_3 forms and evolves along the device over the course of the catalyst's life with different sulfation levels. Even though the NH_3 formation mechanism is not yet clearly understood, there are several general features observed by several research groups. For example, NH_3 generally increases with higher reductant concentrations and lower temperatures [17,20,21]. Another notable feature is that NH_3 breakthrough begins at late regeneration times coinciding with sharp reductant (H_2 and/or CO) front breakthrough [12,13,15–20,21]. Two conjectured explanations for this late NH_3 appearance are presented in the literature; one suggesting that ''slow storage sites'' are responsible for NH_3 formation and the other suggesting NH_3 is an active intermediate that results in nitrate reduction to N_2.

According to the first explanation for late NH_3 appearance, the long tailing NH_3 peak indicates the existence of storage sites that release NO_x more slowly than others, and these slow sites are responsible for ammonia formation [13,16–18,21]. For example, NO_x stored on Ba sites far from precious metals could be more difficult to release than that stored proximal to precious metals sites and could therefore survive until late regeneration times [18]. The resulting high reductant/NO_x ratio at such late regeneration times would favor NH_3 formation [17]. However, NH_3 measurements generally suffer significant instrumental temporal broadening (e.g., due to NH_3 sticking to instrument walls) which confounds interpreting literature data regarding the extent to which ''slow NO_x release sites'' were responsible for the seconds-long NH_3 tail observed during fast cycling where the rich pulse is only 2–5 s [15–17]. Despite these experimental limitations, NH_3 data from slow lean/rich cycling experiments (e.g., minutes-long) appear to at least partly support the existence of ''slow NO_x release sites'' [12,13,17,18,21].

The second explanation for late NH_3 appearance is based on the observation that NH_3 is an effective reductant for the regeneration of $Pt/Ba/Al_2O_3$ [19] and its late appearance has been explained by progressive consumption of NH_3 (produced at upstream locations) by downstream stored nitrates [19,20]. Such intermediate NH_3 formation and consumption by NO_x is yet to be demonstrated experimentally.

In our previous study of a commercial LNT with oxygen storage capacity (OSC) [23], we found that sulfation led to a significant increase in NH_3 selectivity at 325 °C. Measuring species and temperature transients directly inside/along the catalyst, we showed that the NSR reactions occur primarily over a relatively short zone (''NSR zone'') at the upstream end of the monolith, and that sulfation poisons NO_x storage sites progressively in a plug-like manner beginning from the upstream end as well. One of the consequences of sulfation is thus a progressive downstream displacement of the NSR zone and a resultant shortening of the zone where primarily oxygen storage occurs (''OSC-only zone'') located downstream of the NSR zone. Shortening this OSC-only zone reduces the capacity of the catalyst to oxidize NH_3 formed within and slipping from the NSR zone. Thus, we tentatively concluded that reduced oxidation of NH_3 in the OSC-only zone was responsible for the increased NH_3 breakthrough with sulfation.

Expanding this approach [23] to a broader temperature range and performing postmortem catalyst characterization, the objective of the present work was to improve our understanding of how global LNT performance is related to the intra-catalyst distribution of reactions. In the following, we will show that the global performance trends observed as a function of temperature and sulfur loading can be rationalized in a consistent way based on information regarding the axial distribution of, and the interplay between, relevant LNT reactions.

2. Experimental

A bench-flow reactor was used in this study to sulfate, desulfate and evaluate a commercial gasoline direct injection (GDI) LNT manufactured by Umicore (washcoated honeycomb cordierite monolith; 97 cells per cm^2). According to semi-quantitative metals screening with inductively coupled plasma-mass spectrometry (ICP-MS) performed at Galbraith Laboratories, Inc. (Knoxville, Tennessee), the catalyst contains magnesium, aluminum, cerium, zirconium, and barium as major components. Other elements of significance were platinum, palladium, rhodium, lanthanum, iron, and titanium. The total surface area of the degreened sample (cordierite substrate + washcoat) was determined to be 27.1 $m^2\ g^{-1}$ by N_2 adsorption using the BET method. More details on this catalyst can be found in other publications [17,21,23–25]. The 2.1-cm diameter and 7.4-cm long core, taken from the original LNT

monolith and evaluated in our previous work [23], was further analyzed in this study. The sample was wrapped in Zetex insulation tape and inserted into a horizontal quartz reactor tube (2.2-cm inside diameter). The reactor tube was heated by an electric furnace, and simulated exhaust gas mixtures were prepared using pressurized gas bottles (ultra high purity grade, Air Liquide). The gases were metered with mass flow controllers (Unit Instruments Series 7300, Kinetics Electronics) and pre-heated before entering the quartz reactor. Water was introduced by a peristaltic cartridge pump (Cole-Parmer) to a heated zone, vaporized and added to the simulated exhaust mixture. A rapid switching 4-way valve system was used to alternate between the lean and rich gas mixtures so that the lean/rich and rich/lean transitions in these experiments were almost instantaneous (e.g., within 0.2 s). Two K-type thermocouples were placed outside the LNT (1-mm diameter, at ca. 0.6 cm axially from the monolith faces) and one K-type thermocouple (0.25-mm diameter) was translated inside a monolith channel to monitor transient temperature profiles at different locations. The gas composition was analyzed in situ either at the reactor outlet or inside the reactor/catalyst. At the reactor outlet (or inlet by using a bypass gas line), two heated chemiluminescent detectors (California Analytical Instruments, 400-HCLD) measured NO and NO_x concentrations and an FT-IR gas analyzer (Midac M2000) measured NO_2, N_2O, NH_3, CO, CO_2, and H_2O. Intra-catalyst gas phase speciation was performed by using spatially resolved capillary inlet mass spectrometer (SpaciMS) developed in house [16,23,26–28]. The mass spectrometer, equipped with a magnetic-sector mass filter, allowed quantitative measurement of H_2 ($m/z = 2$) as well as total NO_x ($m/z = 30$), H_2S ($m/z = 34$) and SO_2 ($m/z = 48$). A minimally invasive capillary inlet system (sampling rate: ca. 10 μL min^{-1}, probe size: ca. 150-μm outside diameter) was employed to transport time-varying species pools to the mass spectrometer for analysis. A capillary probe was introduced from the reactor inlet near the centerline and positioned at different catalyst locations: just before the LNT inlet; 1/4, 1/2, and 3/4 of the LNT length; and just after the LNT outlet.

Realistic lean/rich cycling conditions were used to study the catalyst NSR and OSC functions (see Table 1). The cycle timing used was 60-s lean and 5-s rich. In addition to their specific constituents, both the lean- and rich-phase species pools contained 5% H_2O, 5% CO_2 and N_2 balance. The rich phase contained 3.4% H_2 with zero NO and O_2. In the NSR mode, the lean phase contained 300 ppm NO and 10% O_2. In the OSC mode, the lean phase contained zero NO and 10% O_2. OSC-attributable H_2 consumption during the rich phase could be quantified (to determine ''effective OSC'': OSC available under given cycling conditions) via OSC-mode operation. We observed with FT-IR CO slipping from the catalyst during OSC measurements due to reverse water–gas shift reaction as our feed contained 5% CO_2. However, its contribution to the global H_2 consumption was negligible under our experimental conditions (i.e., 0–1% of the total H_2 input). Hydrogen consumption in the NSR mode was due to the combined effects of the NSR and OSC functions. NSR-attributable H_2 consumption was determined from the difference in the H_2 consumption measured in the NSR and OSC modes. Thus, tracking H_2 consumption trends allows the various catalyst functions to be probed separately (within the limits of measurement error). Specifically, the distributed nature of OSC- and NSR-attributable H_2 consumption is indicative of the spatially distributed nature of the OSC and NSR functions, respectively.

Table 1
Details of the NO_x (and oxygen) storage/reduction cycling experiment

Environment	Lean	Rich
Duration (s)	60	5
Temperature (°C)	200, 325, and 400	200, 325, and 400
Space velocity (h^{-1})	30,000	30,000
NO (ppm)	300 or 0[a]	0
O_2	10%	0%
H_2	0%	3.4%
H_2O	5%	5%
CO_2	5%	5%
N_2	Balance	Balance

[a] For oxygen storage/reduction experiments.

The catalyst performance with respect to NSR and OSC were evaluated at 200, 325, and 400 °C with different sulfur loadings. Prior to the initial baseline unsulfated-state evaluation at each temperature, the catalyst had been through several sulfation–desulfation cycles to establish steady performance; desulfation was achieved by temperature-programmed reduction with a temperature ramp to 700 °C. Thus, the catalyst had been exposed to this high temperature and performance-stabilizing conditions prior to evaluation. After the initial evaluation (0 g S L^{-1}: 0 g sulfur loading per liter LNT), sulfur was loaded by adding 40 ppm SO_2 into the feed stream for 1 h (1.7 g S L^{-1}) while continuously cycling between lean and rich conditions at 400 °C. Following sulfur exposure, the system was allowed to equilibrate for at least 0.5 h under lean/rich cycling without SO_2. No significant NO_x breakthrough profile change was observed during this purging period. After the initial sulfation and 0.5-h purge, the catalyst performance was evaluated with respect to NSR and OSC at the different temperatures to assess the impact of sulfur loading. Subsequently, another identical 40-ppm SO_2 exposure/evaluation cycle was carried out (3.4 g S L^{-1} total), followed by NSR and OSC evaluation at the various temperatures. Finally, the catalyst was desulfated and evaluated for NSR and OSC. The desulfation was performed by temperature-programmed reduction in a flowing mixture of 0.1% H_2, 5% H_2O, 5% CO_2, balance N_2 (space velocity = 30,000 h^{-1}). The temperature of the furnace was raised from 400 to 700 °C at 5 °C min^{-1} and then maintained at 700 °C for ca. 1 h. Following the desulfation and subsequent performance evaluation, the sample was sulfated again, for postmortem analyses, by flowing 40 ppm SO_2 for 2 h (3.4 g L^{-1}) according to the procedure described above.

For catalyst characterization, the sulfated sample was sliced, perpendicular to the catalyst length, into four equal segments and each segment was sliced into two equal pieces along the catalyst length. One half from each of the four axial LNT

segments was ground and used for elemental analyses performed at Galbraith Laboratories Inc. Inductively coupled plasma-atomic emission spectrometry (ICP-AES) was employed for Pt, Pd, Rh, Ba, and Ce measurements and a combustion non-dispersive infrared (NDIR) method was used to quantify S content. The relative standard deviations of the measurements were estimated to be 10 and 2.1%, respectively, for the ICP-AES and combustion-NDIR methods.

The second half of each axial LNT segment was used for diffuse reflectance infrared Fourier transform spectroscopy (DRIFTS) experiments. A wafer one monolith channel thick was cut from the flat side of each segment. These wafers, measuring approximately 20-mm long by 20-mm wide by 1-mm thick, were loaded onto a bidirectional translation stage. The translation stage was integrated into the DRIFTS apparatus, which consists of a Midac M2500 spectrometer coupled with a Harrick Barrel Ellipse Diffuse Reflectance/Emission Sampling Terminal. All sample spectra were collected at ambient temperature and pressure under room air and at 2-cm^{-1} resolution. Spectra were collected at 1-mm intervals along the axis of each wafer. To convert the sample single beam spectra into absorbances, we collected a background spectrum on an unsulfated wafer of the same catalyst. The unsulfated wafer (measuring approximately 10 mm by 10 mm by 1-mm thick) was loaded into a stainless steel heated reaction cell. It was cycled overnight at 350 °C (10-min lean: 300 ppm NO, 10% O_2, balance Ar; 10-min rich: 0.5% H_2, balance Ar) to drive off carbonates; reduced at 500 °C under 0.5% H_2 for 0.5 h; and then cooled under 100% Ar to 50 °C where the background spectrum was collected.

3. Results

3.1. Global NO_x conversion and N_2O and NH_3 selectivities determined from reactor-outlet measurements

Fig. 1 presents the global NO_x conversion and N_2O and NH_3 selectivities as a function of temperature and sulfur loading. At each evaluation condition (i.e., sulfur loading and temperature), lean/rich cycling was performed for at least 2 h. Data were taken after 1 h of cycling when the catalyst performance stabilized to a fixed limit cycle. The NO_x conversion and NH_3 and N_2O selectivities were obtained by averaging over five consecutive cycles and defined as

$$\text{NO}_x\ \text{conversion}\ (\%) = \frac{\text{total NO}_x\ \text{input} - \text{total NO}_x\ \text{breakthrough}}{\text{total NO}_x\ \text{input}} \times 100 \quad (1)$$

$$\text{NH}_3\ (\text{or N}_2\text{O})\ \text{selectivity}\ (\%) = \frac{\text{total NH}_3\ (\text{or } 2\text{N}_2\text{O})\ \text{breakthrough}}{\text{total NO}_x\ \text{input} - \text{total NO}_x\ \text{breakthrough}} \times 100 \quad (2)$$

where total NO_x, NH_3 or N_2O breakthrough values in ppm-s were determined from chemiluminescent and FT-IR gas analyzer measurements by integrating over the lean/rich cycle.

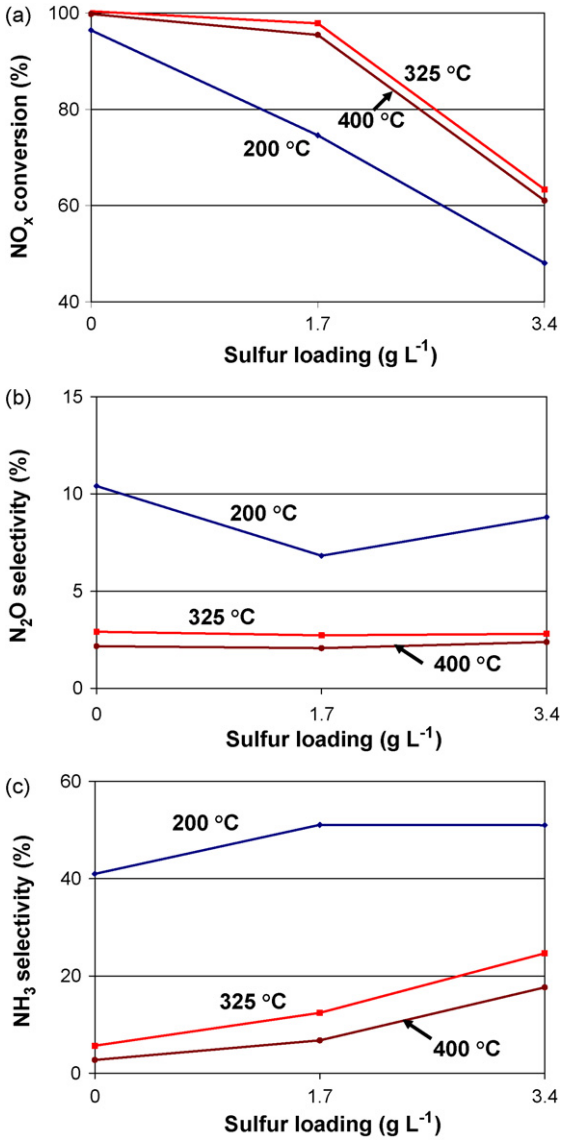

Fig. 1. Cycle-averaged lean NO_x trap performance as a function of sulfur loading and temperature: (a) NO_x conversion, (b) N_2O selectivity, and (c) NH_3 selectivity. Calculations were based on the breakthrough profiles measured at the reactor outlet by chemiluminescent (NO_x) and FT-IR (N_2O and NH_3) analyzers.

In the unsulfated state, the catalyst showed high NO_x conversion at all temperatures (96% at 200 °C and 100% at 325 and 400 °C as shown in Fig. 1a). With the first 1.7 g L^{-1} sulfur dosing, NO_x conversion dropped significantly (to 75%) at 200 °C but was still greater than 95% at 325 and 400 °C. The second 1.7 g L^{-1} sulfur dosing (totaling 3.4 g L^{-1}) further degraded the 200-°C NO_x conversion to 48% and significantly decreased the conversion at 325 and 400 °C. At both 1.7 and 3.4 g L^{-1} sulfur loadings, the NO_x conversion was slightly higher at 325 than 400 °C and significantly higher than 200 °C.

Fig. 1b summarizes the N_2O selectivity trends. Overall N_2O increased at lower temperatures, but was relatively low for all conditions (2–10%). N_2O selectivity showed no meaningful trend as a function of sulfur loading. In contrast, the NH_3 selectivity increased significantly with sulfation, and the effect

was greater at 325 and 400 °C compared to that at 200 °C (Fig. 1c). Indeed, while NH_3 selectivity continuously increased with each 1.7 g L^{-1} sulfur dosing at 325 and 400 °C, at 200 °C NH_3 selectivity increased only slightly with the first dosing and remained virtually unchanged with the second dosing. With respect to the temperature effect, NH_3 selectivity increased significantly with decreasing temperature.

3.2. Axial distribution of hydrogen consumption

Hydrogen utilization during the 5-s regeneration phase of NSR- and OSC-mode cycling experiments was assessed by SpaciMS to study temperature and sulfur impacts on the distribution of local reactions. The raw H_2 data are not shown here, but representative profiles can be found in our previous paper [23]. Briefly, these raw profiles show the temporal distribution of H_2 at each sample location, and the H_2 utilization during early regeneration times at different catalyst locations. The temporal profiles were averaged over two or three cycles and the net H_2 at each location (ppm-s) was determined by integrating the H_2 profiles over the averaged cycle. The cumulative H_2 utilization at a given intra-catalyst location, temperature, sulfur loading and operating mode (NSR or OSC) was determined by using the corresponding integrated values; here we represent cumulative H_2 utilization as a percentage of total integrated inlet hydrogen for the corresponding run, and calculate its value for each location through the catalyst:

$$\text{Cumulative } H_2 \text{ utilization } (\%) = \frac{\text{total } H_2 \text{ input} - \text{total } H_2 \text{ breakthrough}}{\text{total } H_2 \text{ input}} \times 100 \quad (3)$$

Measurements during OSC showed the distributed H_2 utilization due to oxygen storage/reduction (Fig. 2). Likewise, measurements in the NSR mode indicated distributed H_2 utilization due to the combined effect of NSR and OSC (Fig. 3). To determine the NSR-attributable H_2 utilization during NSR-mode cycling, the hydrogen profiles in the OSC mode were subtracted from those in the NSR mode (Fig. 4). We observed some fluctuations in the regeneration pulse that could impact our calculations. Specifically, measurements at different locations, sulfur loadings, temperatures, and operating modes were taken at different times, and relied on a repeatable regeneration pulse. We measured some fluctuations in this regeneration pulse which could be observed by variations in the inlet H_2 profiles at the various sulfur loadings, temperatures, and operating modes. These variations were not systematic, and their impact was mitigated by cycle averaging. We characterized the uncertainty in our data associated with these fluctuations based on the standard deviation of the mean of all inlet H_2 profiles from our experiments, and by propagating this value through the data reduction equations. Accordingly, the uncertainty in the calculated cumulative NSR- and OSC-mode hydrogen utilization is 3% based on 2-sigma, and that for the NSR-attributable H_2 consumption is 6%. The corresponding uncertainty is shown via the bars on the data obtained at 1.7 g L^{-1} sulfur loading but applies to all curves in Figs. 2–4.

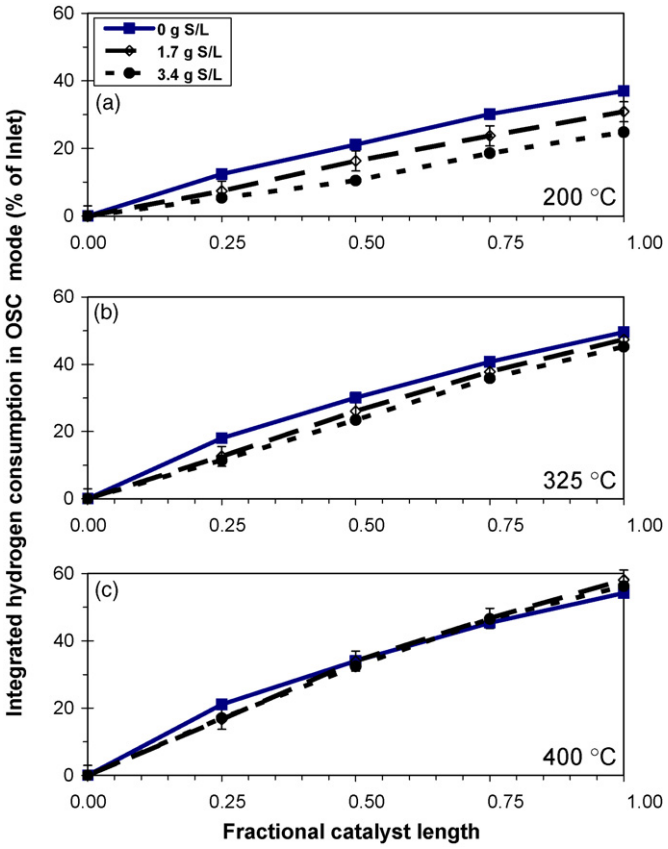

Fig. 2. Axial distribution of total H_2 consumption as a function of sulfur loading during oxygen-storage-capacity cycling at (a) 200 °C, (b) 325 °C, and (c) 400 °C.

As shown in Fig. 2, the evaluated LNT had significant OSC uniformly distributed along its length. OSC increased significantly with temperature from 200 to 325 °C and to a lesser extent from 325 to 400 °C. Sulfation in general decreased the OSC, but its impact decreased with increasing temperature and was barely quantifiable at 400 °C. From the 200 and 325 °C data (Fig. 2), it can be seen that the OSC degradation associated with the first sulfur dosing was confined to the first quarter of the LNT; this is most apparent for the 200 °C data where the H_2-consumption curves are parallel over the back 3/4 of the catalyst for the 0- and 1.7-g S L^{-1} cases. The second sulfur dosing further degraded the first-quarter OSC to some extent and significantly degraded that in the second quarter. Thus, the progression of the sulfation front from the first and second quarters of the catalyst with the first and second sulfur dosings can be followed. It is notable that even after the second sulfur dosing the first and second catalyst quarters maintained significant OSC, especially at high temperatures; i.e., the advancing sulfation zone in the catalyst front did not completely poison OSC in that same region. Furthermore, the back catalyst portion beyond the sulfated zone maintained its initial OSC capacity as indicated by the unchanging curve slopes with sulfation.

Compared to OSC, NSR-attributable H_2 consumption was more axially localized, particularly at higher temperatures (Fig. 4); this is consistent with our previous observations of the localized nature of NSR [23]. We note that Fig. 4 needs to be interpreted with some caution since the subtraction operation

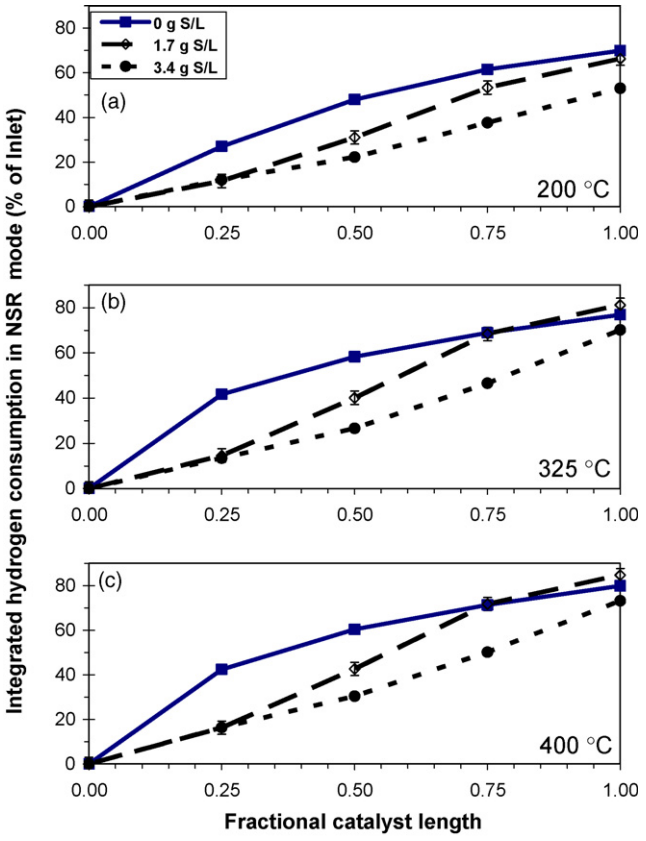

Fig. 3. Axial distribution of total H_2 consumption as a function of sulfur loading during NO_x storage/reduction cycling at (a) 200 °C, (b) 325 °C, and (c) 400 °C.

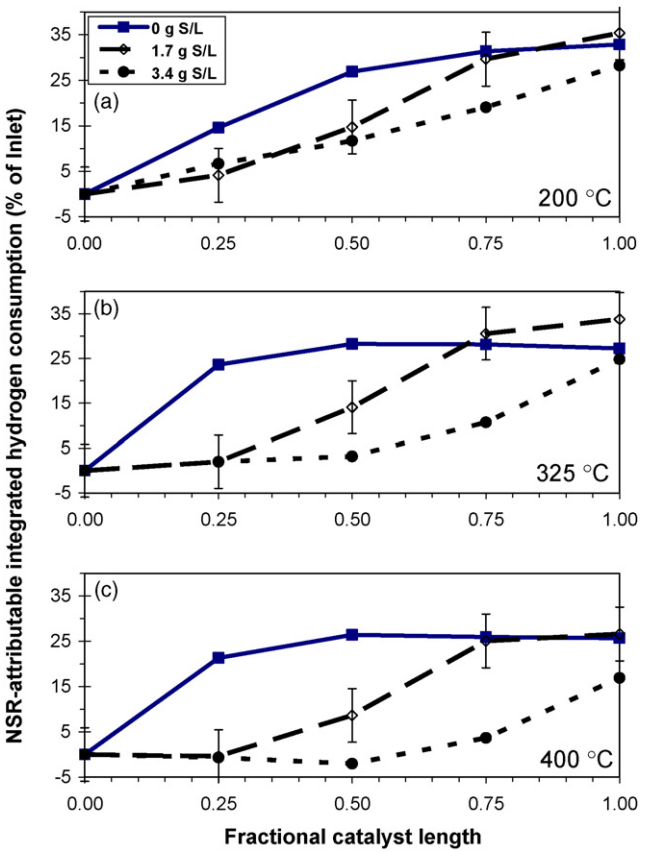

Fig. 4. Axial distribution of NSR-attributable H_2 consumption as a function of sulfur loading during NO_x storage/reduction cycling at (a) 200 °C, (b) 325 °C, and (c) 400 °C.

(NSR − OSC) used to obtain NSR-attributable H_2 consumption assumes that NSR and OSC sites were mutually exclusive; i.e., there would be some error in the NSR-attributable H_2 consumption if the secondary function of the NSR and OSC sites (O_2 and NO_x storage, respectively) impacted their primary function. Moreover, it is important to note that NSR-attributable H_2 consumption is the sum of H_2 consumed to reduce NO_x to N_2, N_2O, and NH_3, and thus conditions favoring high NH_3 selectivity stoichiometrically resulted in more H_2 consumption per unit of NO_x reduced. Total H_2 conversion calculated based on the global NO_x conversion and N_2O and NH_3 selectivities reported in Fig. 1 agrees with the H_2 data measured at the catalyst outlet (Fig. 4) within our experimental error. Overall, the 325 and 400 °C data indicate similar axial distribution of NSR as a function of sulfur loading (Fig. 4). In the unsulfated state, the NSR-attributable H_2 consumption was confined mainly to the first quarter of the LNT with minor additional consumption in the second quarter. No measurable NSR-attributable H_2 consumption occurred over the back catalyst half indicating insignificant lean-phase NO_x storage in this region. After dosing 1.7 g L^{-1} sulfur, NSR-attributable H_2 consumption mainly occurred in the second and third quarters, with negligible reactivity in the first and last quarters. With 3.4 g L^{-1} sulfur dosing, the NSR-attributable H_2 consumption was practically absent in the first half of the LNT and mainly occurred in the back half. The NSR-attributable H_2 consumption took place over a significantly longer portion of the LNT at 200 °C than at the higher temperatures (Fig. 4). Indeed, at 200 °C NSR-attributable H_2 consumption occurred throughout the catalyst even at 0 g L^{-1} sulfur loading. Also unique to the 200 °C case was apparent NSR activity in the sulfated zone; specifically, although NSR-attributable H_2 consumption decreased significantly in the first quarter with the first sulfur dosing, and in the second and third quarters with the second sulfur dosing, small but measurable consumption persisted in the sulfated zone. The apparently increased H_2 consumption at 200 °C in the first quarter going from 1.7 to 3.4 g L^{-1} sulfur loadings is well within the experimental uncertainty.

3.3. Elemental analysis of the axial segments of a sulfated LNT

Table 2 summarizes the bulk chemical composition of the four equal-length segments of the LNT core with 3.4 g L^{-1} sulfur loading. Each segment contained a similar amount of Pt, Pd, Rh, Ba, and Ce. In fact, there is a slight composition variation along the length (the loadings generally decreasing from the first through the last quarters) but it falls within the measurement uncertainty. On the contrary, the total sulfur content differed significantly and decreased continually from the first through the last quarter. While the total sulfur decreased linearly from the first through third quarter, the decrease was noticeably greater from the third to the last

Table 2
Data obtained from elemental analysis of a commercial LNT loaded with 3.4 g L^{-1} sulfur

LNT segment no.[a]	Pt[b] (%)	Pd[b] (%)	Rh[b] (%)	Ba[b] (%)	Ce[b] (%)	S[c] (%)	S/Ba (mol/mol)	S/Ce (mol/mol)	S associated with NO_x storage sites[d] (%)	S associated with OSC[e] (%)
1	0.447	0.140	0.055	2.875	11.900	1.225	1.82	0.45	0.672	0.553
2	0.438	0.138	0.053	2.525	12.050	0.903	1.53	0.33	0.590	0.313
3	0.422	0.134	0.050	2.550	11.700	0.647	1.09	0.24	0.596	0.051
4	0.419	0.133	0.051	2.530	11.800	0.201	0.34	0.07	0.201	0.000

[a] An LNT core was sliced into four equal-length segments (1 and 4 designate first and fourth quarters, respectively).
[b] Measured by ICP-AES.
[c] Measured by combustion method.
[d] Estimated assuming that sulfur was preferentially associated with barium until all barium was sulfated with a stoichiometry of S:Ba = 1:1.
[e] Estimated assuming that the remainder of sulfur after total barium sulfation was associated with OSC.

quarter. Considering the Ba content of each segment and the theoretical maximum S/Ba ratio (i.e., 1), it is obvious that a significant portion of the total sulfur was associated with components other than Ba. However, our data indicating complete NSR poisoning but only OSC degradation in the sulfation zone (i.e., stronger affinity of S to Ba than to OSC as will be discussed in Section 4) is consistent with preferential sulfation of Ba sites. Therefore, for any segment containing more S than necessary to sulfate all Ba atoms, we assumed that Ba was sulfated first and then the remaining sulfur was associated with the OSC component (mainly Ce). Based on this assumption, Fig. 5 shows a distinct step change in S associated with NSR sites (mainly Ba sites) between the third and last quarter, while there is a more progressive decrease in S associated with OSC sites. We hasten to note that while the trends in Fig. 5 seem reasonable, they depend on our assumption that Ba is preferentially sulfated before Ce. This assumption still needs to be verified via atomic-scale physicochemical characterization.

3.4. DRIFTS analysis of the axial segments of a sulfated LNT

The spectra in Fig. 6 were obtained by analyzing each quarter segment at multiple locations, and present DRIFT features typically found in Ba-based LNTs such as Ba-sulfates (1350–1000 cm^{-1} region) [8,29–34] and Ba carbonates (1550–1350 cm^{-1} region) [8,29–34]. OSC-associated bulk and surface sulfates are known to be located in the Ba-sulfate and Ba-carbonate regions, respectively [8,35]. We need more work to verify the Ce-associated features, and separate the individual Ce and Ba contributions in the broad 1350–1000 cm^{-1} region. The broad feature found at 1450 cm^{-1} in the front LNT portion is yet to be identified. The relative intensity of the peaks due to sulfates and carbonates differed significantly along the LNT length. Sulfates were dominant in the front portion of the catalyst, with little indication of Ba-carbonates. The amount of sulfates remained approximately constant until catalyst midpoint, and then decreased significantly in the catalyst back half with a corresponding increase in Ba-carbonates. The peak near 1640 cm^{-1} and the concomitant broad peak at 3490 cm^{-1} was due to water bound to the catalyst surface (probably on alumina [30,31,33]), as we confirmed experimentally (results not shown). Note that these two water-related peaks closely followed the peaks assigned to Ba-sulfates: they remained high with little change from the inlet through roughly half of the LNT, and then decreased along the remaining length. Though significantly smaller, the sulfate- and water-associated features persisted in the back end of the LNT.

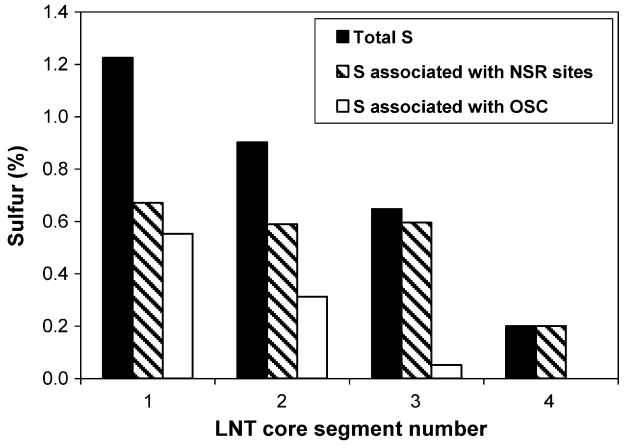

Fig. 5. Axial distribution of sulfur estimated from elemental analysis of a commercial LNT loaded with 3.4 g L^{-1} sulfur. The core segment number 1 of the *x*-axis designates the first quarter while 4 designates the fourth quarter of the LNT sample studied.

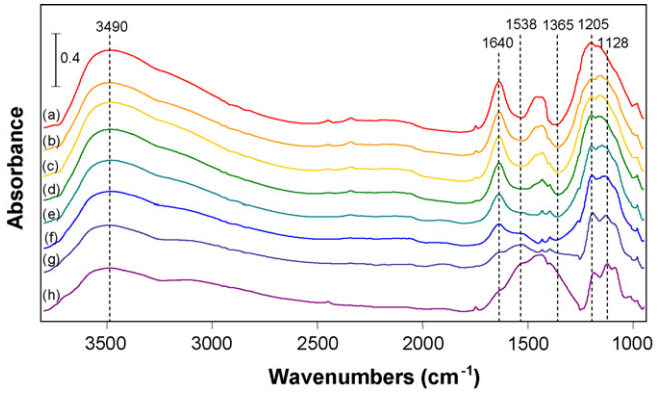

Fig. 6. DRIFT spectra obtained at different axial locations of a commercial LNT loaded with 3.4 g L^{-1} sulfur; fractional position = (a) 0.08, (b) 0.20, (c) 0.32, (d) 0.45, (e) 0.57, (f) 0.68, (g) 0.80, and (h) 0.92.

4. Discussion

4.1. Axial distribution of NO_x and oxygen storage/reduction as a function of temperature and sulfur loading

The results in Section 3 show that the spatial distribution of the various reactions depended on reaction temperature and sulfur loading. A conspicuous aspect of our data is the significantly different NSR axial distribution at 200 °C compared to 325 and 400 °C. From the NSR-attributable H_2 consumption trends (Fig. 4), it is clear that NO_x storage/reduction was localized at 325 and 400 °C but considerably more distributed at 200 °C. A wider NSR zone at 200 °C is indicative of requiring a greater length of catalyst to achieve an equivalent global NO_x conversion and thus less efficient use of the catalyst. It is known that intrinsic NO_x storage capacity, determined by hour-long lean exposure, is higher at a lower temperature due to the favorable thermodynamic stability of nitrates [3,36]. However, effective capacity governs lean/rich cycling performance and generally follows a volcano-type dependence on temperature with a maximum around 300 °C due to the most favorable combination of NO oxidation rate, nitrate formation rate, nitrate stability, and regeneration rate [3]. Our measurements are not able to partition the origin of the degraded low-temperature efficiency among these processes.

Another conspicuous aspect of our data is the axial uniformity of OSC compared to the localized NSR. As the oxygen storage component (Ce) was distributed evenly along the catalyst (Table 2) and 10% oxygen was present during the lean phase of the cycling, the uniformly distributed OSC-attributable H_2 consumption profiles in Fig. 2 were expected. The effective OSC was lower at a lower temperature, indicating lower reduction rate during the rich-phase of the cycling.

The NSR and OSC functions had very different responses to sulfation. Recalling that the spatial distribution of NSR-attributable H_2 utilization indicates that of the NSR function, Fig. 4 demonstrates that the unsulfated-state NSR occurred mainly in the catalyst front region, and that this localization was more pronounced for the higher temperatures compared to that at 200 °C. As sulfation progressed, the front portion became effectively inactive for NO_x storage and the catalyst NSR zone was displaced downstream. This plug-like inhibition of NSR and effective poisoning of NSR in the sulfated zone was observed in our previous study at 325 °C with sulfation performed at 325 °C [23] (cf. 400 °C sulfation used in this study) and is in good agreement with the axial distribution of Ba-associated sulfur estimated by elemental (Fig. 5) and DRIFTS (Fig. 6) analyses. On the contrary, the sulfation of OSC was more distributed (Fig. 2) and fewer OSC sites were sulfated compare to NSR sites (Table 2); i.e., significant OSC remained active in the sulfated zone [23]. In previous studies on commercial LNTs, Rohr et al. claimed no significant sulfation of OSC components [31,32], however, considering the bulk S/Ba less than unity determined in their study (i.e., milder sulfation than used here), our claim of OSC sulfation is not contradictory. The observed higher sensitivity of sulfur to Ba than to OSC is reasonable considering the more basic nature of alkaline earth metal oxides, typical NO_x storage components [4,5]. We can conjecture that there was a sulfation front moving in a plug-like manner axially dividing sulfated and unsulfated Ba, and that the OSC upstream of that front was less efficiently sulfated thus resulting in axially varying Ce sulfation state.

It is notable that sulfation led to increased exposure of the alumina support. As described in Section 3, the DRIFT spectra in Fig. 6 show a peak at 1640 cm^{-1}, which has been attributed to water associated with the alumina support [30,31,33]. This peak shows a trend very similar to that of the sulfate features in the 1350–1000 cm^{-1} region: its magnitude is fairly constant in the first half of the LNT, and it decreases in the second half. This trend indicates that more of the alumina support was exposed in the front half of the catalyst. We attribute the increased alumina exposure to barium particle growth resulting from sulfation (evolution from surface to bulk sulfates with increasing sulfur dosing was reported elsewhere [29,33]). The sulfur to barium ratio of 1 in the front region of the LNT (i.e., complete sulfation; Table 2, Fig. 5) appears to be consistent with the virtually unchanging peak intensity at 1640 cm^{-1} in this same region (i.e., maximum Ba particle coarsening was achieved at the reaction conditions employed). Therefore, monitoring the peak at 1640 cm^{-1} could be a good method for evaluating the extent of barium sulfation. However, we admit that due to the complex nature of the fully formulated catalyst used here, more study, especially using different characterization tools such as microscopy and XPS, is necessary to confirm particle growth with sulfation and associated alumina support exposure.

In addition to the wide NSR zone at 200 °C described above, there are some additional sulfation-response features specific to 200 °C. For example, NSR-attributable H_2 consumption was observed in the sulfated zone (Fig. 4). As sulfation of Ba was complete in the front region (Table 2, Fig. 5), this apparent discrepancy appears to be attributable to the NO_x storage ability of the OSC catalyst component. Recently, Ji et al. showed that ceria-addition to $Pt/Ba/Al_2O_3$ enhances NO_x storage capacity, especially at low temperatures [37]. Our elemental analysis data show that S/Ce was well below unity even at 3.4 g L^{-1} sulfur loading (Table 2). Another outstanding feature of the cycling at 200 °C is a greater inhibition of OSC upon sulfation (Fig. 2) compared to the higher temperatures. We do not have a clear explanation at this time but it should also be noted that, even though there is a systematic trend with temperature, the observed changes were within the experimental error as discussed in Section 3.

4.2. Rationalization of the global LNT performance trends on the basis of axial distribution of reactions

Taking into account the axial sulfur distribution arising from sulfation and the associated evolution of the NSR and OSC distributions at different temperatures, we can explain the observed global performance trends (Fig. 1) in a consistent manner. The cartoon in Fig. 7 was prepared to help understand correlations between spatial distribution of reactions and global performance. The enhanced degradation in NO_x conversion at 200 °C compared to 325 and 400 °C for each sulfation level is attributable to the length of catalyst necessary for efficient

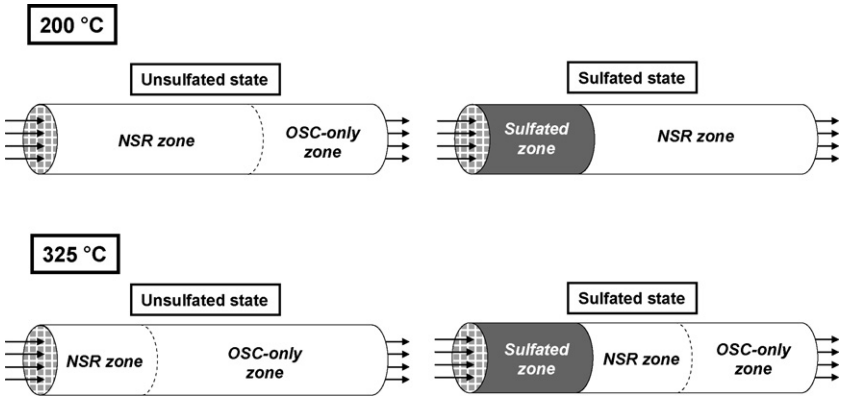

Fig. 7. Pictorial representation of the distribution of reactions inside a commercial lean NO_x trap during fast lean/rich cycling at 200 and 325 °C before and after sulfation at 400 °C.

NSR. As a much wider NSR zone was necessary at 200 °C than at 325 and 400 °C to achieve an equivalent conversion (see the unsulfated-state performance in Figs. 1, 4 and 7), the impact of plug-like Ba sulfation was much more profound at 200 °C. Specifically, even the downstream displacement of the NSR zone associated with the first 1.7 g L^{-1} sulfur loading resulted in a remaining unsulfated LNT length shorter than what was required to achieve a high conversion at 200 °C, resulting in significant NO_x breakthrough (see the sulfated-state performance in Figs. 1, 4 and 7). On the contrary, more extensive sulfur poisoning of the LNT was necessary to observe noticeable impact on the outlet NO_x breakthrough due to a much shorter or more localized NSR zone at 325 and 400 °C. In general, NO_x breakthrough was not observed as long as the NSR zone was less than the catalyst length available downstream of the sulfated zone. And, in operating conditions where the NSR zone was localized, greater degrees of sulfation and corresponding greater downstream displacement of the NSR zone was necessary to observe NO_x breakthrough.

In terms of N_2O selectivity, sulfation had little effect and produced no meaningful trend. This insensitivity might be due to the fact that N_2O measured at the reactor outlet was formed inside the NSR zone without being consumed later downstream. If N_2O had been a product of NH_3 (formed in NSR zone) oxidation by OSC or NO_x, for example, sulfation would have decreased N_2O selectivity since sulfation shortened the OSC-only zone available downstream of the NSR zone. Alternatively, if N_2O had been a product of NO_x reduction in the NSR zone and could have been further reduced to N_2 or NH_3 downstream of the NSR zone by residual reductant, sulfation would have increased N_2O selectivity.

The conceptual model we proposed to explain the NH_3 trend for cycling at 325 °C [23] appears to be applicable to lower and higher temperatures. The NH_3 selectivity response to sulfation was very similar for 325 and 400 °C, and so were the corresponding spatial reaction distributions. As sulfation displaced the NH_3-forming NSR zone downstream, the downstream OSC-only zone where NH_3 oxidation took place was shortened and, consequently, NH_3 breakthrough increased. Recently, Parks et al. studied the same catalyst used here in a full engine-system [38]. From FT-IR analysis of the gas sampled through small holes made on the catalyst side, they observed that NH_3 increased and then decreased along the catalyst under certain operating conditions. This observation suggests that our conceptual model [23] may be applicable to complex real exhaust conditions. The slightly higher NH_3 selectivity at 325 °C than at 400 °C at each sulfation level could have been due to slightly higher local H_2/NO_x ratio at 325 °C resulting from lower local NO_x release rate. Increasing NO_x release rate with temperature was reported for the same catalyst recently by Epling et al. [21]. Alternatively, the higher NH_3 selectivity at 325 °C could have been due to higher effective OSC at 400 °C. That is, more NH_3 could have been consumed by OSC instantly inside the NSR zone or in the downstream OSC-only zone. The remarkably high NH_3 selectivity obtained at 200 °C could also be related at least in part to the slow rate of NO_x release. In addition, as the NSR zone was wider at this temperature (i.e., less NO_x stored in a given length of the LNT), the local H_2/NO_x ratio had to be higher than that at 325 and 400 °C. Another potential contributor to the increased NH_3 selectivity is low effective OSC at 200 °C. Either within the NSR zone or in the OSC-only zone, less NH_3 would have been oxidized by OSC at 200 °C. Finally, at 200 °C the OSC-only zone was practically non-existent (see Fig. 7) and thus afforded little possibility for oxidizing NH_3 slipping from the NSR zone.

From this discussion, it is clear that a precise understanding of the spatial distribution of reactions is an important element in developing a model which can reliably predict LNT outlet NO_x, N_2O and NH_3 breakthrough over a broad range of sulfation levels and temperatures. In particular, such a model should take into account the local NO_x release rate, effective OSC, NSR-zone width, location of the NSR zone, and the OSC-only zone width to accurately predict NH_3 selectivity.

5. Conclusions

We found that the global performance trends of a commercial lean NO_x trap as a function of temperature (200, 325, and 400 °C) and sulfur loading (0, 1.7, and 3.4 g L^{-1}) could be consistently explained based on changes in the axial distributions of three characteristic reaction zones: a sulfated zone, an NSR zone, and an OSC-only zone. Key specific observations were:

- In the unsulfated state, a high NO_x conversion was achieved within the front half of the LNT at 325 and 400 °C (shorter NSR zone and longer OSC-only zone), but almost the entire LNT length was required at 200 °C (longer NSR zone and shorter or non-existent OSC-only zone).
- In the unsulfated state, oxygen storage/reduction took place relatively uniformly along the entire LNT length at all temperatures and effective oxygen storage capacity increased with temperature.
- Sulfur poisoned NO_x and oxygen storage sites progressively with increasing sulfur loading beginning at the catalyst front edge (growing sulfated zone). NO_x storage sites were more effectively poisoned than oxygen storage sites resulting in a more plug-like axial poisoning of the NO_x storage/reduction function. However, NO_x storage-site poisoning was axially less distinct at 200 °C compared to that at 325 and 400 °C; this is likely due to the significant NO_x storage ability of unsulfated oxygen storage components at low temperatures.
- Global NO_x conversion decreased significantly at 200 °C with sulfur loading while it did so only at high sulfur loading at 325 and 400 °C. This higher sensitivity to sulfation at 200 °C appeared to result from the fact that even slight axial progression of the sulfation front made the length of the downstream unsulfated zone shorter than that necessary to achieve high conversion.
- Global NH_3 selectivity increased with decreasing temperature and increasing sulfur loading. In addition, the sulfation impact on NH_3 was much higher at 325 and 400 °C than at 200 °C. We propose that these trends can be explained by lower NO_x release rates combined with diminishment of the OSC-only zone, thereby reducing the opportunity for NH_3 to be oxidized before exiting the reactor.
- Reactor-outlet N_2O selectivity was generally low (2–10%). Selectivity was higher at lower temperature but showed no meaningful trend with sulfur loading. These results suggest insignificant downstream reaction of N_2O formed in, and slipping from, the NSR zone.

We expect that the important axial reaction variations identified in this study will be useful in developing a reliable LNT reactor model which can predict LNT performance over a broad range of temperatures and sulfation levels.

Acknowledgements

This research was sponsored by the US Department of Energy, Office of Vehicle Technologies, with Ken Howden and Gurpreet Singh as the Program Managers. We thank Mr. Owen Bailey of Umicore for assistance in obtaining the commercial LNT catalyst used in these experiments and also CLEERS LNT Focus Group members for useful discussions.

References

[1] E. Jobson, Top. Catal. 28 (2004) 191.
[2] M.V. Twigg, Appl. Catal. B 70 (2007) 2.
[3] W.S. Epling, L.E. Campbell, A. Yezerets, N.W. Currier, J.E. Parks II, Catal. Rev. Sci. Eng. 46 (2004) 163.
[4] N. Miyoshi, S. Matsumoto, K. Katoh, T. Tanaka, J. Harada, N. Takahashi, K. Yokota, M. Sugiura, K. Kasahara, SAE Technical Paper 950809 (1995).
[5] N. Takahashi, H. Shinjoh, T. Iijima, T. Suzuki, K. Yamazaki, K. Yokota, H. Suzuki, N. Miyoshi, S. Matsumoto, T. Tanizawa, T. Tanaka, S. Tateishi, K. Kasahara, Catal. Today 27 (1996) 63.
[6] M. Takeuchi, S. Matsumoto, Top. Catal. 28 (2004) 151.
[7] R.C. Yu, A.S. Cole, B.J. Stroia, S.C. Huang, K. Howden, S. Chalk, SAE Technical Paper 2002-01-1867, 2002.
[8] H. Mahzoul, L. Limousy, J.F. Brilhac, P. Gilot, J. Anal. Appl. Pyrol. 56 (2000) 179.
[9] J. Li, J. Theis, W. Chun, C. Goralski, R. Kudla, J. Ura, W. Watkins, M. Chattha, R. Hurley, SAE Technical Paper 2001-01-2503, 2001.
[10] S. Poulston, R.R. Rajaram, Catal. Today 81 (2003) 603.
[11] S. Elbouazzaoui, E.C. Corbos, X. Courtois, P. Marecot, D. Duprez, Appl. Catal. B 61 (2005) 236.
[12] L. Castoldi, I. Nova, L. Lietti, P. Forzatti, Catal. Today 96 (2004) 43.
[13] J. Parks, S. Huff, J. Pihl, J.-S. Choi, B. West, SAE Technical Paper 2005-01-3876, 2005.
[14] M. Swartz, S. Huff, J. Parks, B. West, SAE Technical Paper 2006-01-3423, 2006.
[15] R.G. Tonkyn, R.S. Disselkamp, C.H.F. Peden, Catal. Today 114 (2006) 94.
[16] J.-S. Choi, W.P. Partridge, W.S. Epling, N.W. Currier, T.M. Yonushonis, Catal. Today 114 (2006) 102.
[17] J.A. Pihl, J.E. Parks II, C.S. Daw, T.W. Root, SAE Technical Paper 2006-01-3441, 2006.
[18] I. Nova, L. Castoldi, L. Lietti, E. Tronconi, P. Forzatti, Top. Catal. 42/43 (2007) 21.
[19] L. Cumaranatunge, S.S. Mulla, A. Yezerets, N.W. Currier, W.N. Delgass, F.H. Ribeiro, J. Catal. 246 (2007) 29.
[20] A. Lindholm, N.W. Currier, E. Fridell, A. Yezerets, L. Olsson, Appl. Catal. B 75 (2007) 78.
[21] W.S. Epling, A. Yezerets, N.W. Currier, Appl. Catal. B 74 (2007) 117.
[22] H. Hu, J. Reuter, J. Yan, J. McCarthy Jr., SAE Technical Paper 2006-01-3552, 2006.
[23] J.-S. Choi, W.P. Partridge, C.S. Daw, Appl. Catal. B 77 (2007) 145.
[24] R.S. Larson, V.K. Chakravarthy, J.A. Pihl, C.S. Daw, SAE Technical Paper 2006-01-3446, 2006.
[25] W.S. Epling, A. Yezerets, N.W. Currier, Catal. Lett. 110 (2006) 143.
[26] W.P. Partridge, J.M.E. Storey, S.A. Lewis, R.W. Smithwick, G.L. DeVault, M.J. Cunningham, N.W. Currier, T.M. Yonushonis, SAE Technical Paper 2000-01-2952, 2000.
[27] B.H. West, S.P. Huff, J.E. Parks, S.A. Lewis, J.-S. Choi, W.P. Partridge, J.M. Storey, SAE Technical Paper 2004-01-3023, 2004.
[28] J.-S. Choi, W.P. Partridge, C.S. Daw, Appl. Catal. A 293 (2005) 24.
[29] Ch. Sedlmair, K. Seshan, A. Jentys, J.A. Lercher, Catal. Today 75 (2002) 413.
[30] C. Courson, A. Khalfi, H. Mahzoul, S. Hodjati, N. Moral, A. Kiennemann, P. Gilot, Catal. Commun. 3 (2002) 471.
[31] F. Rohr, S.D. Peter, E. Lox, M. Kögel, A. Sassi, L. Juste, C. Rigaudeau, G. Belot, P. Gélin, M. Primet, Appl. Catal. B 56 (2005) 201.
[32] F. Rohr, U. Göbel, P. Kattwinkel, T. Kreuzer, W. Müller, S. Philipp, P. Gélin, Appl. Catal. B 70 (2007) 189.
[33] H. Abdulhamid, E. Fridell, J. Dawody, M. Skoglundh, J. Catal. 241 (2006) 200.
[34] M.A. Peralta, V.G. Milt, L.M. Cornaglia, C.A. Querini, J. Catal. 242 (2006) 118.
[35] M. Waqif, P. Bazin, O. Saur, J.C. Lavalley, G. Blanchard, O. Touret, Appl. Catal. B 11 (1997) 193.
[36] T.J. Toops, D.B. Smith, W.P. Partridge, Catal. Today 114 (2006) 112.
[37] Y. Ji, T.J. Toops, M. Crocker, Catal. Lett. 119 (2007) 257.
[38] J. Parks, S. Huff, M. Swartz, B. West, Presented at the 10th DOE Crosscut Lean Exhaust Emissions Reduction Simulations (CLEERS) Workshop, Dearborn, MI, May 2, 2007 (http://www.cleers.org/workshops/workshop10/presentations/Parks_CLEERS_10.pdf).